

1 **On the semi-annual formation of large scale**
2 **three-dimensional vortices at the stratopause**

3 **Terence J. O’Kane¹, Vassili Kitsios², Mark A. Collier²**

4 ¹CSIRO Oceans and Atmosphere, Battery Point, Hobart, Tasmania, Australia

5 ²CSIRO Oceans and Atmosphere, Aspendale, Melbourne, Victoria, Australia

6 **Key Points:**

- 7 • EOF analysis of the second matrix invariant of the velocity gradient tensor is ap-
8 plied to the shear zones about the tropical stratosphere.
9 • We identify large scale vortices near the tropical stratopause as reconstructed in
10 the NASA MERRA-2 atmospheric reanalysis.
11 • The vortices form following the vernal and autumnal equinoxes at times where the
12 westerley jet is maximal.

Corresponding author: Terence J. O’Kane, terence.okane@csiro.au

Abstract

An examination of the dynamics of the middle atmosphere as reconstructed in the NASA Modern-Era Retrospective analysis for Research and Applications, Version 2 (MERRA-2) reveals the formation of large scale three dimensional vortices in the tropical stratosphere following both the vernal and autumnal equinoxes at times where the jet associated with the westerly phase of the semi-annual oscillation (SAO) is maximal and extratropical influences from planetary waves are weakest. An empirical orthogonal function (EOF) analysis of the second matrix invariant of the velocity gradient tensor applied to the shear zones about the SAO reveals statistically stationary wave-5 vortex structures that span more than 3200km in length and up to 40km in the vertical. Eliassen-Palm fluxes suggests the vortices are maintained by a combination of local (shear zones) and remote (vertically propagating tropical) sources of momentum. These large scale coherent features appear to be unique to the stratopause.

Plain Language Summary

Application of methods commonly employed in engineering fluid mechanics to visualise vortices are used to examine a recent state of the art reconstruction of the middle atmosphere. This analysis reveals huge vortical structures present during the equinoctial seasons in the region of the tropical stratopause. These semi-annual coherent features appear to be unique to the middle atmosphere spanning up to 30° longitude at ±15° latitude corresponding to around 3200km in length and between 10hPa and 0.1hPa encompassing up to 40km in the vertical.

1 Introduction

The tropical middle atmosphere semiannual oscillation (SAO), observed in temperature and the zonal wind variations, was first discovered in radiosonde and rocketsonde measurements in the early 1960's (R. J. Reed, 1962). The SAO is evident from the upper levels of the stratosphere (stratopause) and throughout the mesosphere with very clear phase-locking to the annual cycle. The SAO dominates the variability about the stratopause ($\approx 1\text{hPa}$) where easterly extreme wind speeds are typically reached following the December and June solstices and the westerly extreme winds after the equinoxes around April and October (Müller et al., 1997). The mean annual evolution of the stratopause SAO has been characterised using 20 years of rocketsonde observations at Ascension Island (8°S, 14°W) and Kwajalein (8°N, 167°E) as a Hovmöller time-height diagram of the zonal wind between 20km and 60km in which the westerlies form in the lower mesosphere shortly after the solstices propagating downward with an average speed of 6-7km month⁻¹ and reaching maximum average values in excess of 25ms⁻¹ (20ms⁻¹) after the equinoxes in April (October) (Baldwin et al., 2001). The observed downward progression of the westerly acceleration phase of the SAO suggests a strong role for westerly Kelvin waves as being the source of the requisite momentum flux (R. Reed, 1965), and supported on theoretical grounds in terms of the interaction of a vertically-propagating (Kelvin) wave with the mean (background) flow (Dunkerton, 1979).

Hopkins (1975) first suggested a close coupling between the easterly phase of the SAO and planetary wave activity in the winter hemisphere arguing that, consistent with the theoretical work of Dickinson (1968), the stationary planetary waves of the winter hemisphere stratosphere would be absorbed about the critical line i.e., where the mean zonal wind is 0ms⁻¹, near the equator producing an easterly zonal acceleration with little tendency for downward propagation. Hopkins (1975) further suggested that the stronger planetary wave activity in the Northern Hemisphere winter was the cause for the stronger variance in the monthly mean easterly tropical zonal winds after the January solstice ($\approx 40\text{ms}^{-1}$) in contrast to the June solstice ($\approx 20\text{ms}^{-1}$). On the basis of Hopkins (1975) study, Holton (1975) proposed that the SAO results from the combined effects of a steady back-

63 ground source of westerly momentum due to Kelvin waves excited in the tropical tro-
64 posphere as the cause of the westerly phase of the SAO where its downward propaga-
65 tion is indicative of dissipation of vertically propagating waves near critical layers. In con-
66 trast, the easterly phase was hypothesised to arise from an oscillating source of easterly
67 momentum due to vertically and equatorward propagating planetary waves of the win-
68 ter hemisphere stratosphere being absorbed near the critical line in the tropics.

69 Subsequent observational studies added further weight to the mechanism proposed
70 by Holton (1975), showing that the transition from westerlies to easterlies occurs rather
71 suddenly throughout a deep layer due to the easterly phase of the SAO being forced by
72 the dissipation of horizontally traveling planetary waves (Hirota, 1980) and cross-equatorial
73 advection of easterly winds by the residual mean meridional circulation (R. J. Reed, 1966;
74 Meyer, 1970; Holton & Wehrbein, 1980; Dickinson, 1968; Meyer, 1970; van Loon et al.,
75 1972; Belmont et al., 1974a, 1974b; Hopkins, 1975; Müller et al., 1997; Garcia et al., 1997;
76 Garcia & Sassi, 1999; Hirota, 1978, 1980; Li et al., 2012)). Additional observational stud-
77 ies of temperature and trace constituent data (Hirota, 1978, 1979; Bergman & Salby, 1994),
78 combined with analysis based on the vertical component of the Eliassen-Palm (E-P) flux
79 (Andrews et al., 1983), revealed short-period, equatorially trapped Kelvin waves with
80 periods less than 2 days propagating vertically into the stratosphere are the most likely
81 sources of the majority of the momentum required to generate both the quasi-biennial
82 oscillation (QBO) and SAO (see also Sato and Dunkerton (1997)). Bergman and Salby
83 (1994) used high resolution imagery of the global convective pattern to show that these
84 short period waves are generated in geographical locations over the Indian Ocean to the
85 western tropical Pacific and to a lesser extent over the African, and American continents.
86 The change of SAO phase is in part due to mean meridional advection of momentum as
87 air is advected towards the winter pole. A recent detailed analysis of the momentum bud-
88 get in the stratosphere, mesosphere, and lower thermosphere has been undertaken by Sato
89 et al. (2018) and Yasui et al. (2018).

90 The structure of descending alternating easterly and westerly jets comprising the
91 SAO and their associated shear zones suggests the possibility that large scale coherent
92 structures might form at times where the vertical easterly - westerly - easterly jet struc-
93 ture is sufficiently strong that the shear zones above and below the westerly jet might
94 join to form vortical filaments. The main methods for the identification of three dimen-
95 sional vortices are based on pointwise analysis of the velocity gradient tensor (Chakraborty
96 et al., 2005). The characteristic shapes of vortical structures in turbulent flows, includ-
97 ing regions of vorticity in the form of filaments, sheets, and blobs are a question of long-
98 standing and intense interest. Vortex filaments are known to play an important role in
99 the overall turbulence dynamics where local or point-wise methods of vortex identifica-
100 tion typically are used to define a function that can be evaluated point-by-point and then
101 classify each point as being inside or outside a vortex according to a criterion based on
102 the point values (Hunt et al., 1988; Chong et al., 1990; Soria et al., 1994; Kitsios et al.,
103 2011). Most local vortex identification criteria are based on the kinematics implied by
104 the velocity gradient tensor, thereby making them Galilean invariant. One of the most
105 popularly used local criteria is the second matrix invariant of the velocity gradient ten-
106 sor Q (Hunt et al., 1988). In order to isolate regions that might contain coherent vortical
107 structures, we first calculate the velocity gradient tensor from the MERRA-2 re-
108 analysis (Gelaro & Co-authors, 2017), then, following Soria et al. (1994), we calculate
109 Q between 100hPa and 0.01hPa. Empirical orthogonal function (EOF) analysis is then
110 applied to isolate regions of high Q variance and the corresponding vortical (positive Q)
111 isosurface structures.

112 This paper is structured as follows. The MERRA-2 reanalysis is briefly described
113 in section 2. We next characterise the SAO as represented in MERRA-2 in section 3 fol-
114 lowed by the calculation of the velocity gradient tensor and the second invariant Q (sec-

tion 4.1, and the EOFs of Q (section 4.2) and a case study of the observed vortical structures evident on April 1984 (section 4.3). A final summary is presented in section 5.

2 Data

We analyse the middle atmosphere using MERRA-2 data. MERRA-2 is an atmospheric reanalysis of the modern satellite era produced by the NASA Global Modeling and Assimilation Office (GMAO) (Gelaro & Co-authors, 2017). The processed daily and monthly averages used in this study are based on 3-hourly time averaged three-dimensional collections consisting of 361 latitudes, 576 longitudes and 72 levels. The height - pressure relationship to model level is displayed in (supplemental Figure 1). All analyses are performed on the full horizontal grid with calculations of the vortex structures restricted to the 38 levels above 100hPa. MERRA-2 provides a multidecadal reanalysis whereby aerosol and meteorological (satellite radiances, microwave temperature, ATOVs etc) observations are jointly assimilated within a global data assimilation system. In addition to improved representations of cryospheric processes, MERRA-2 also includes several improvements to the representation of the stratosphere including ozone (total column, profiles from EOS Aura OMI). Importantly for the middle atmosphere, the gravity wave parameterization has been retuned to produce a model generated QBO rather than relying on one imposed through reanalysis tendencies to the wind and temperature fields. For a complete list of observations assimilated see table 1 of Gelaro and Co-authors (2017). Of relevance to our study, in the stratosphere at 10hPa MERRA-2 has a negative bias of 20.3 Kelvin (K°) prior to the assimilation of AIRS radiances in 2002. These biases trend upward becoming positive in 2005. After 2005, assimilation of both MLS temperature retrievals (above 5hPa) and GPSRO bending angle observations (up to approximately 10hPa) begins in MERRA-2 such that after 2006, the biases have an average value of 0.2-0.3 K. Importantly for this study MERRA-2, resolves most of the middle atmosphere up to just below the mesopause at 0.01hPa. We will not discuss MERRA-2 further simply referring the reader to the relevant citation (Gelaro & Co-authors, 2017). MERRA-2 products are accessible online through the NASA Goddard Earth Sciences Data Information Services Center (GES DISC).

3 Characterising the semi-annual oscillation in MERRA-2

In the following we summarise the general mechanism of the SAO easterly and westerly phases, as present in MERRA-2, in terms of the propagation of zonal winds over time and via the transfer of momentum. Figure 1 shows monthly averages of the U zonal winds averaged between 0° - 360° longitude and 5° N- 5° S latitude. The black contour shows zero average of winds. April and October are indicated by the pink and cyan vertical lines respectively. The downward propagation of the alternating easterly and westerly jets is evident as are their relative strengths.

Eliassen-Palm (E-P) fluxes are calculated to examine the transfer of momentum from sources in the extratropics via the winter hemisphere and also tropical sources due to Kelvin and inertial gravity waves. The E-P flux provides a useful tool to describe wave propagation in mean zonal shear flows (Andrews et al., 1983). The E-P flux is defined as

$$\mathbf{F} = \{F_\phi, F_p\} = \left\{ -a \cos \phi \overline{U'V'}, f a \cos \phi \frac{\overline{V'\theta'}}{\theta_p} \right\} \quad (1)$$

where a is the Earth's radius, f is the Coriolis effect, ϕ is the latitude, θ the potential temperature, the zonal and meridional velocities (U, V). Eddy flux terms are computed from the daily zonal anomalies and the product is zonally and then time averaged over the period 1980-2019. $\theta_p = \frac{\partial \theta}{\partial p}$ is calculated as the time-mean, zonal mean value of θ . When the E-P flux vector points upward, the meridional heat flux dominates; when the vector points in the meridional direction, the meridional flux of zonal momentum dominates.

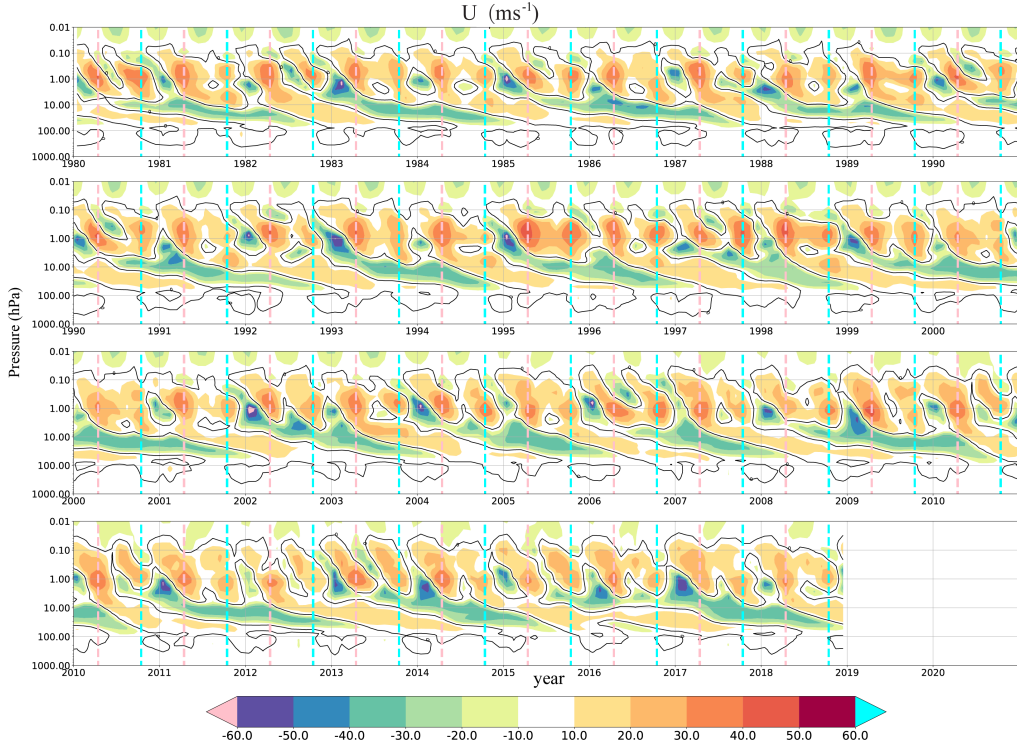


Figure 1. Monthly averages of the U zonal winds averaged between 0° - 360° longitude and 5° N- 5° S latitude. Black contour shows zero average of winds. April and October are indicated by the pink and cyan vertical lines respectively.

164
165

The divergence of the E-P flux is proportional to the eddy potential vorticity flux and when zero i.e. $\nabla \cdot \mathbf{F} = 0$, thermal wind balance is maintained (Edmon et al., 1980).

166
167
168
169
170
171
172
173
174
175
176

Climatological E-P fluxes were calculated using daily U, V and θ data over the period 1980-2018 (see supplemental Figure 2). In Figure 2 shading is the flux divergence with negative values (red) indicating absorption and positive (blue) shading indicative of production of momentum. Black contours are the climatological winds whereas the critical line corresponds to the magenta contour line. All quantities (E-P fluxes and U zonal winds) have been divided (normalised) by the associated 1980-2018 standard deviation at each latitude and level. This has the two-fold benefit of 1) not requiring the usual ad-hoc scaling of quantities in the vertical, for example due to the magnitude differences of E-P flux vector components and 2) highlighting exceptional values e.g. individual months or years as discussed in the following sections. In addition, the vectors below 100hPa have been appropriately thinned for display purposes.

177
178
179
180
181
182
183
184
185
186

For the easterly SAO phase, the Hovmöller plot of the MERRA-2 zonal winds U in the middle atmosphere reveals the relative strengths of the easterly SAO maxima following the respective solstices (Figure 1). Specifically, the maximum zonal winds are in excess of 30ms^{-1} and occur in January and August at $\approx 1\text{hPa}$ following the December and June solstices. In January, the easterly jet is at a maximum then decays as it propagates downward over the first half of the year before re-establishing with typically significantly weaker maximum values after the June solstice. Climatological E-P flux vectors during the solstices (supplemental Figure 2) reveal extratropical planetary waves propagating into the tropics from the winter hemisphere whereas E-P flux divergences show deposition of (easterly) momentum due to the dissipation of the aforementioned

187 planetary waves driving wave forcing and mean advection. This is consistent with the
 188 general mechanism for the easterly phase of the SAO first proposed by Holton (Holton,
 189 1975). Additional E-P fluxes indicative of possible nonlinear advection of easterly mean
 190 momentum by the summer to winter mean meridional circulation may also contribute
 191 to maintain the easterly phase (Holton & Wehrbein, 1980). As the SAO easterly phase
 192 relies on planetary wave forcing and mean momentum advection, it is strongly coupled
 193 to the annual cycle and specifically to the winter hemisphere. The strong zonal asym-
 194 metry arises due to the injection of momentum from the winter hemisphere, hence the
 195 easterly phase of the SAO is structurally unable to support the existence of large scale
 196 coherent vortices.

197 The westerly phase (Figure 1) is characterised by a pronounced zonal symmetry
 198 about the equator and strong mean westerly jets in excess of 35ms^{-1} . For the months
 199 of April and October immediately after the equinoxes, the westerly SAO jet, centered
 200 near 1 hPa, is maximal with zonally symmetric momentum fluxes and divergence (Fig-
 201 ure 2). E-P flux divergence is positive where the equatorial jet forms acting to maintain
 202 and enhance the jet. Note that the jet associated with easterly phase of the quasi-biennial
 203 oscillation (Coy, Wargan, et al., 2017; Coy, Newman, et al., 2017) is seen centered at 10
 204 hPa. The E-P fluxes indicate the equatorial regions are the primary source of momen-
 205 tum driving the westerly equatorial stratopause jet, with little evidence of systematic
 206 momentum flux due to extratropical planetary waves. Tropical sources due to Kelvin and
 207 inertial gravity waves are clearly evident during the westerly phase. These sources of mo-
 208 mentum are associated with tropical convection and are thought to be responsible for
 209 generating the westerly phase via interaction of the mean flow with vertically propagat-
 210 ing internal gravity waves and large-scale equatorial waves generated in the lower atmo-
 211 sphere. The climatological westerly jet has a generally downward propagation from 0.1hPa
 212 to about 1hPa and is strongest in April with a secondary maxima in October. Our re-
 213 sults are generally supportive of the hypothesis of Holton (1975) that high frequency Kelvin
 214 waves, with periods from 2 to 4 days, originating in the troposphere propagate unhin-
 215 dered into the middle atmosphere where they are absorbed about the critical line as the
 216 major source of momentum during the westerly phase.

217 4 Stratopause vortex structures

218 An examination of the middle atmosphere Q in all months (not shown) revealed
 219 vortical structures are only evident in the stratopause SAO westerly phase and are most
 220 coherent after the equinoxes. These structures are highly dependent on the westerly jet
 221 being sufficiently strong, requiring velocities in excess of 35ms^{-1} , and where sufficient
 222 shear is present in the gradients at the upper and lower boundaries of the SAO. We shall
 223 show that preferential conditions for these vortex structures to occur are where there is
 224 a well developed easterly jet present in the vicinity of 0.1hPa above the westerly SAO
 225 jet and when the QBO is strongly easterly.

226 4.1 Calculation of Q

227 Following (Chong et al., 1990; Soria et al., 1994; Chakraborty et al., 2005) we de-
 228 fine the velocity gradient tensor A_{ij} in terms of symmetric $S_{ij} = S_{ji}$ and anti-symmetric
 229 $W_{ij} = -W_{ji}$ parts where,

$$230 \quad A_{ij} = \partial u_i / \partial x_j = S_{ij} + W_{ij} \quad (2a)$$

231 and

$$232 \quad S_{ij} = (\partial U_i / \partial x_j + \partial U_j / \partial x_i) / 2 \quad (2b)$$

$$233 \quad W_{ij} = (\partial U_i / \partial x_j - \partial U_j / \partial x_i) / 2 \quad (2c)$$

234 are the rate of strain and the rate of rotation tensors respectively. The $U_{i=1,2,3}$ indices
 235 are the zonal and meridional velocities (U, V) in meters per second (ms^{-1}) and ω the

236 Lagrangian rate of change of pressure with time in units of pascals per second ($Pa\ s^{-1}$).
 237 The $x_{i=1,2,3}$ indices are latitude and longitude (ϕ, λ) in meters (m) and isobaric pres-
 238 sure level p in Pa respectively. The eigenvalues γ of A_{ij} satisfy the characteristic equa-
 239 tion

$$240 \quad \gamma^3 + P\gamma^2 + Q\gamma + R = 0, \quad (2d)$$

241 where the matrix invariants are

$$242 \quad P = -\text{Tr}[A] = -S_{ii} \quad (2e)$$

$$243 \quad Q = \frac{1}{2}(P^2 - \text{Tr}[A^2]) = \frac{1}{2}(P^2 - S_{ij}S_{ji} - W_{ij}W_{ji})$$

$$244 \quad = \begin{vmatrix} \frac{\partial U}{\partial \phi} & \frac{\partial U}{\partial \lambda} \\ \frac{\partial V}{\partial \phi} & \frac{\partial V}{\partial \lambda} \end{vmatrix} + \begin{vmatrix} \frac{\partial U}{\partial \omega} & \frac{\partial U}{\partial p} \\ \frac{\partial \omega}{\partial \phi} & \frac{\partial \omega}{\partial p} \end{vmatrix} + \begin{vmatrix} \frac{\partial V}{\partial \lambda} & \frac{\partial V}{\partial p} \\ \frac{\partial \omega}{\partial \lambda} & \frac{\partial \omega}{\partial p} \end{vmatrix} \quad (2f)$$

245 Tr is the trace, Q has units of s^{-2} , and

$$246 \quad R = -|A| \quad (2g)$$

247 where $||$ defines the determinant.

248 For turbulence in three dimensional flows, large scale coherent eddies decay as vorticity
 249 diffuses out in convergence zones defined where there is irrotational straining and
 250 strong divergence and convergence of streamlines. In other words, the magnitude of the
 251 straining defined by $S_{ij}S_{ji}$ is large compared to the magnitude of the rate of rotation,
 252 with regions of elongation $S_{ij}S_{jk}S_{ki} > 0$ and flattening $S_{ij}S_{jk}S_{ki} < 0$ (Hunt et al.,
 253 1988). For incompressible flows, where the first flow invariant $P = -S_{ii} = 0$, it fol-
 254 lows that the second invariant $Q = (W_{ij}W_{ij} - S_{ij}S_{ij})/2$. This means that large nega-
 255 tive values of Q are indicative of regions where the strain dominates the rotation whereas
 256 for large positive values rotation dominates strain. In the results presented here, we have
 257 defined Q in terms of the zonal and meridional velocities (U, V) and ω the Lagrangian
 258 rate of change of pressure with time therefore, the interpretation of Q is exactly as for
 259 3D turbulence.
 260

261 4.2 EOFs of Q

262 In calculating EOFs of Q , we first construct daily anomalies w.r.t. the climatolog-
 263 ical month i.e. $Q'(\phi, \lambda, p, t) = Q(\phi, \lambda, p, t) - \bar{Q}(\phi, \lambda, p)$. We then construct spatial anom-
 264 alies from the zonal average as $Q''(\phi, \lambda, p, t) = Q'(\phi, \lambda, p, t) - Q'(\lambda, p, t)$. These anom-
 265 alies are then normalized by the spatial and temporal standard deviation σ of Q'' at each
 266 pressure level i.e. $\hat{Q}(\phi, \lambda, p, t) = Q''(\phi, \lambda, p, t)/\sigma(p)$. In the current study, vortex struc-
 267 tures will be represented by isosurfaces of EOFs of Q . Normalizing by the spatio-temporal
 268 standard deviation allows us to then rescale the EOF patterns before calculating the iso-
 269 surfaces of interest i.e. $Q_i^{eof}(\phi, \lambda, p) = \hat{Q}_i^{eof}(\phi, \lambda, p) \times \sigma(p)$.

270 The 3D structures for the leading EOFs 1 & 2 of Q for April (Figure 3) and Oc-
 271 tober (Figure 4) reveal a distinct wave-5 pattern with opposite sign about the equator
 272 due to the change of sign in the meridional velocity gradient. These EOFs are in quadra-
 273 ture. The corresponding April 2D EOFs at 0.62hPa i.e., through the middle of the westerly
 274 jet, have explained variances of 2.9% and 2.4% respectively. The structures are less
 275 coherent between 200°E and 300°E which is the region where the westerly jet of the SAO
 276 is consistently weak and where the mean zonal wind velocities, are considerably less than
 277 the maximum mean values as indicated by the $35ms^{-1}$ mean U contour line (yellow) in
 278 the top-down perspectives. As for April, the leading pair of 3D-EOFs of October Q are
 279 confined to a region where the background zonal U wind exceeds $35ms^{-1}$. The struc-
 280 tures would again appear to be close to a hemispheric wave-5 pattern if the westerly jet
 281 was strong enough to support it.

282 The April 3D-EOFs 3 & 4 (supplemental figure 3) form a large scale wave-4 pat-
 283 tern with individual structures in excess of 40° longitude spanning 20°N to 20°S . The
 284 corresponding 2D-EOFs 3 & 4 explain 2.3% & 2.0% of the Q variance respectively at
 285 0.62hPa. All 4 leading 3D-EOFs for April display noticeable asymmetry being larger and
 286 more coherent south of the equator. October 3D EOFs 3 & 4 (supplemental Figure 4)
 287 appear to be wave-6 and again do not display the North - South asymmetries present
 288 for April. October 3D-EOFs 3 & 4 are considerably noisier than for April, again a re-
 289 flection of the weaker background flow and reduced shear zones. At 0.62hPa, the lead-
 290 ing 4 October 2D-EOFs explain 2.8%, 2.7%, 2.0% & 1.7% of the total explained Q vari-
 291 ance.

292 4.3 April 1984 case study

293 In order to show that the vortical Q structures are not simply statistical, we now
 294 focus exclusively on the westerly phase of the SAO associated and the particular date
 295 of April 1984. This date was chosen as the vortical structures are particularly evident
 296 with no filtering required, however, a number of other dates could have been chosen. An
 297 examination of the mean April 1984 E-P fluxes (figure 5) shows close similarities to the
 298 climatological April previously discussed. Again we see absorption of momentum about
 299 the critical line associated with the easterly QBO phase and some evidence of flux into
 300 the tropics as the SH transitions to winter. There is evidence of eddy forcing (positive
 301 E-P flux divergence) in the shear regions between the easterly QBO and the westerly SAO
 302 ($\approx 10\text{hPa}$), and between the westerly SAO and the weak easterly jet near 0.1hPa . Most
 303 interesting is to consider the anomalous flux w.r.t. the climatological April. Here we see
 304 an intense highly localized source of momentum in the shear zone i.e. +ve E-P flux di-
 305 vergence at 10hPa , with a closeby corresponding region of absorption into the westerly
 306 SAO jet on the opposite side of the critical line between $\pm 20^\circ$ latitude.

307 Having identified the regions of shear between the respective easterly and westerly
 308 jets as significant sources (and sinks) for momentum, we now examine the aforementioned
 309 Q flow invariant. The April 1984 isosurfaces of the monthly mean U winds and Q be-
 310 tween 0.01hPa and 100hPa are shown in figure 6. Here the westerly positive phase of the
 311 SAO (30ms^{-1} green isosurface) is wedged between the easterly mesosphere jet between
 312 0.01hPa and 0.1hPa and the easterly phase of the QBO between 10hPa and 60hPa (5ms^{-1}
 313 purple isosurfaces). In the regions of shear between the respective jets, Q isosurfaces are
 314 largely unorganised and noisy. These are the regions corresponding to large amplitude
 315 anomalous E-P fluxes (figure 5). The large scale coherent positive Q isosurfaces i.e. vor-
 316 tices, are, as for the leading April EOFs, entirely contained within the westerly jet cent-
 317 tred about 1hPa and occur only at latitudes where the jet exceeds 30ms^{-1} . In common
 318 with the April EOFs 1 & 2, these structures span up to 30° longitude at $\pm 15^\circ$ latitude
 319 corresponding to around 3200km in length and between 10hPa and 0.1hPa encompass-
 320 ing up to 40km in the vertical.

321 5 Summary

322 Vortex structures associated with Q manifest only during the SAO westerly phase
 323 and only where the westerly jet reaches speeds in excess of 35ms^{-1} . Similar wind veloc-
 324 ities are necessary to form the shear zones at the jets upper and lower boundary. As such
 325 the vortices are most coherent during March-April and less evident during October. The
 326 Q structures manifest on particular dates with wave numbers between 4-7 but are typ-
 327 ically wave 5, resembling the leading statistically stationary 3D-EOF Q patterns. Our
 328 analysis indicates that the vortices are maintained by a combination of local (shear zones)
 329 and remote (vertically propagating tropical) sources of momentum. Although not directly
 330 discussed here, there is evidence that the phase relationship between the QBO and SAO

331 directly influences the strength of the shear zone at the lower boundary of the stratopause
332 SAO during its westerly phase with consequences for the resulting Q vortices.

333 The emergence of the vortex structures during the westerly SAO phase and their
334 dependence on the jet strength and shear at the boundaries indicates a rich flow geom-
335 etry allowing methods commonly applied to analyse turbulent shear flows to be fruit-
336 fully employed. The scale and extent of these vortical structures, structures that appear
337 to be unique to the stratopause, is remarkable. While the mechanisms of the SAO have
338 been generally understood for quite some time, many of the details remain to be quan-
339 tified, particularly the spectrum of Kelvin and inertial gravity waves required to gener-
340 ate sufficient momentum to drive the westerly phase. Despite not explicitly resolving grav-
341 ity waves due to our reduced temporal resolution, our E-P flux analysis is broadly con-
342 sistent with the recent detailed analysis of Sato et al. (2018). They emphasise the com-
343 plicated roles of E-P flux divergences and nonlinear dynamics during the equinoctial sea-
344 sons, clear motivation for further exploration of the unique coherent structures appear-
345 ing near the stratopause.

346 Acknowledgments

347 The authors appreciate helpful discussions with Adam Scaife and Jorgen S. Frederiksen.
348 We thank Ajay Limaye and support from the NCI Visualisation lab for generating fig-
349 ure 6. This work was supported by the Australian Commonwealth Scientific and Indus-
350 trial Research Organisation (CSIRO) Decadal Climate Forecasting Project (<https://research.csiro.au/dfp>).
351 Datasets for this research are available in these in-text data citation references: (Gelaro
352 & Co-authors, 2017).

353 References

- 354 Andrews, D. G., Mahlman, J. D., & Sinclair, R. W. (1983). Eliassen-Palm diagnos-
355 tics of wave-mean flow interaction in the GFDL "SKYHI" general circulation
356 model. *J. Atmos. Sci.*, *40*, 2768–2784.
- 357 Baldwin, M. P., Gray, L. J., Dunkerton, T. J., Hamilton, K., Haynes, P. H., Randel,
358 W. J., ... Takahashi, M. (2001). The Quasi-Biennial Oscillation. *Reviews of*
359 *Geophysics*, *39*, 179–229.
- 360 Belmont, A. D., Dart, D. G., & Nastrom, G. D. (1974a). Periodic variations in
361 stratospheric zonal wind from 20-65km, at 80°n to 70°s. *Quart. J. Roy. Me-*
362 *teor. Soc.*, *100*, 203–211.
- 363 Belmont, A. D., Dart, D. G., & Nastrom, G. D. (1974b). Variations of stratospheric
364 zonal winds, 20-65 km, 1961-1971. *J. Appl. Meteor.*, *14*, 585–594.
- 365 Bergman, J. W., & Salby, M. L. (1994). Equatorial wave activity derived from fluc-
366 tuations in observed convection. *J. Atmos. Sci.*, *51*, 3791–3806.
- 367 Chakraborty, P., Balachandar, S., & j. Adrian, R. (2005). On the relationships be-
368 tween local vortex identification schemes. *J. Fluid Mech.*, *535*, 189–214. doi:
369 10.1017/S0022112005004726
- 370 Chong, M. S., Perry, A. E., & Cantwell, B. J. (1990). A general classification of
371 three-dimensional flow fields. *Phys. Fluids A.*, *2*, 765–777. doi: 10.1063/1
372 .857730
- 373 Coy, L., Newman, P. A., Pawson, S., & Lait, L. R. (2017). Dynamics of the dis-
374 rupted 2015/16 quasi-biennial oscillation. *J. Clim.*, *30*, 5661–5674.
- 375 Coy, L., Wargan, K., Molod, A. M., McCarty, W. R., & Pawson, S. (2017). Struc-
376 ture and dynamics of the quasi-biennial oscillation in MERRA-2. *J. Climate*,
377 *30*, 5339–5354.
- 378 Dickinson, R. E. (1968). Planetary Rossby waves propagating vertically through
379 weak westerly wind wave guides. *J. Atmos. Sci.*, *25*, 984–1002.
- 380 Dunkerton, T. J. (1979). The role of the Kelvin wave in the westerly phase and the
381 semiannual zonal wind oscillation. *J. Atmos. Sci.*, *36*, 32–41.

- 382 Edmon, H. J., Hoskins, B., & McIntyre, M. (1980). Eliassen-Palm cross sections for
383 the troposphere. *J. Atmos. Sci.*, *37*, 2600–2616.
- 384 Garcia, R. R., Dunkerton, T. J., Lieberman, R. S., & Vincent, R. (1997). Clima-
385 tology of the semiannual oscillation of the tropical middle atmosphere. *J. Geo-
386 phys. Res.*, *102*, 26019–26032.
- 387 Garcia, R. R., & Sassi, F. (1999). Modulation of the mesospheric semiannual oscilla-
388 tion by the quasibiennial oscillation. *Earth Planets Space*, *51*, 563–569.
- 389 Gelaro, R., & Co-authors. (2017). The Modern-Era Retrospective Analysis for Re-
390 search and Applications, Version 2 (MERRA-2). *J. Climate*, *30*, 5419–5454.
391 doi: 10.1175/JCLI-D-16-0758.1
- 392 Hirota, I. (1978). Equatorial waves in the upper stratosphere and mesosphere in re-
393 lation to the semiannual oscillation of the zonal wind. *J. Atmos. Sci.*, *35*, 714–
394 722.
- 395 Hirota, I. (1979). Kelvin waves in the equatorial middle atmosphere observed by
396 Nimbus 5 SCR. *J. Atmos. Sci.*, *36*, 217–222.
- 397 Hirota, I. (1980). Observational evidence of the semiannual oscillation in the tropical
398 middle atmosphere. *Pure Appl. Geophys.*, *118*, 217–238.
- 399 Holton, J. R. (1975). *The dynamic meteorology of the stratosphere and mesosphere*
400 (Vol. 15). American Meteorological Society.
- 401 Holton, J. R., & Wehrbein, W. M. (1980). A numerical model of the zonal mean cir-
402 culation of the middle atmosphere. *Pure Appl. Geophys.*, *118*, 284–306.
- 403 Hopkins, R. H. (1975). Evidence of polar-tropical coupling in upper stratospheric
404 zonal wind anomalies. *J. Atmos. Sci.*, *32*, 712–719.
- 405 Hunt, J. C. R., Wray, A. A., & Moin, P. (1988). Eddies, stream, and convergence
406 zones in turbulent flows. *Proceedings of the Summer Program, Center for Tur-
407 bulent Research Report CTR-S8*, 193–208.
- 408 Kitsios, V., Cordier, L., Bonnet, J.-P., Ooi, A., & Soria, J. (2011). On the coherent
409 structures and stability properties of a leading edge separated aerofoil with
410 turbulent recirculation. *J. Fluid Mech.*, *683*, 395–416.
- 411 Li, T., Liu, A. Z., Lu, X., Li, Z., Franke, S., Swenson, G. R., & Dou, X. (2012).
412 Meteor-radar observed mesospheric semi-annual oscillation (SAO) and quasi-
413 biennial oscillation (QBO) over Maui, Hawaii. *J. Geophys. Res.*, *117*, D05130.
414 doi: 10.1029/2011JD016123
- 415 Meyer, W. D. (1970). A diagnostic numerical study of the semiannual variation
416 of the zonal wind in the tropical stratosphere and mesosphere. *J. Atmos. Sci.*,
417 *27*, 820–830.
- 418 Müller, K. M., Langematz, U., & Pawson, S. (1997). The stratopause semiannual
419 oscillation in the Berlin troposphere-stratosphere-mesosphere GCM. *J. Atmos.
420 Sci.*, *54*, 2749–2759.
- 421 Reed, R. (1965). The quasi-biennial oscillation of the atmosphere between 30km and
422 50km over Ascension Island. *J. Atmos. Sci.*, *22*, 331–333.
- 423 Reed, R. J. (1962). Some features of the annual temperature regime in the tropical
424 stratosphere. *Mon. Weather Rev.*, *90*, 211–215.
- 425 Reed, R. J. (1966). Zonal wind behaviour in the equatorial stratosphere and lower
426 mesosphere. *J. Geophys. Res.*, *71*, 4223–4233. doi: 10.1029/JZ071i018p04223
- 427 Sato, K., & Dunkerton, T. J. (1997). Estimates of momentum flux associated with
428 equatorial kelvin and gravity waves. *J. Geophys. Res.*, *102*, 26247–26261.
- 429 Sato, K., Yasui, R., & Miyoshi, Y. (2018). The momentum budget in the strato-
430 sphere, mesosphere, and lower thermosphere. Part I: Contributions of different
431 wave types and in situ generation of Rossby waves. *J. Atmos. Sci.*, *75*, 3613–
432 3633. doi: 10.1175/JAS-D-17-0336.1
- 433 Soria, J., Sondergaard, R., Cantwell, B. J., Chong, M. S., & Perry, A. E. (1994). A
434 study of the fine-scale motions of incompressible time-developing mixing layers.
435 *Phys. Fluids*, *6*(2), 871–884.

- 436 van Loon, H., Labitzke, K., & Jenne, R. J. (1972). Half-yearly waves in the strato-
437 sphere. *J. Geophys. Res.*, *77*, 3846–3855.
- 438 Yasui, R., Sato, K., & Miyoshi, Y. (2018). The momentum budget in the strato-
439 sphere, mesosphere, and lower thermosphere. Part II: The in situ generation of
440 gravity waves. *J. Atmos. Sci.*, *75*, 3635–3651. doi: 10.1175/JAS-D-17-0337.1

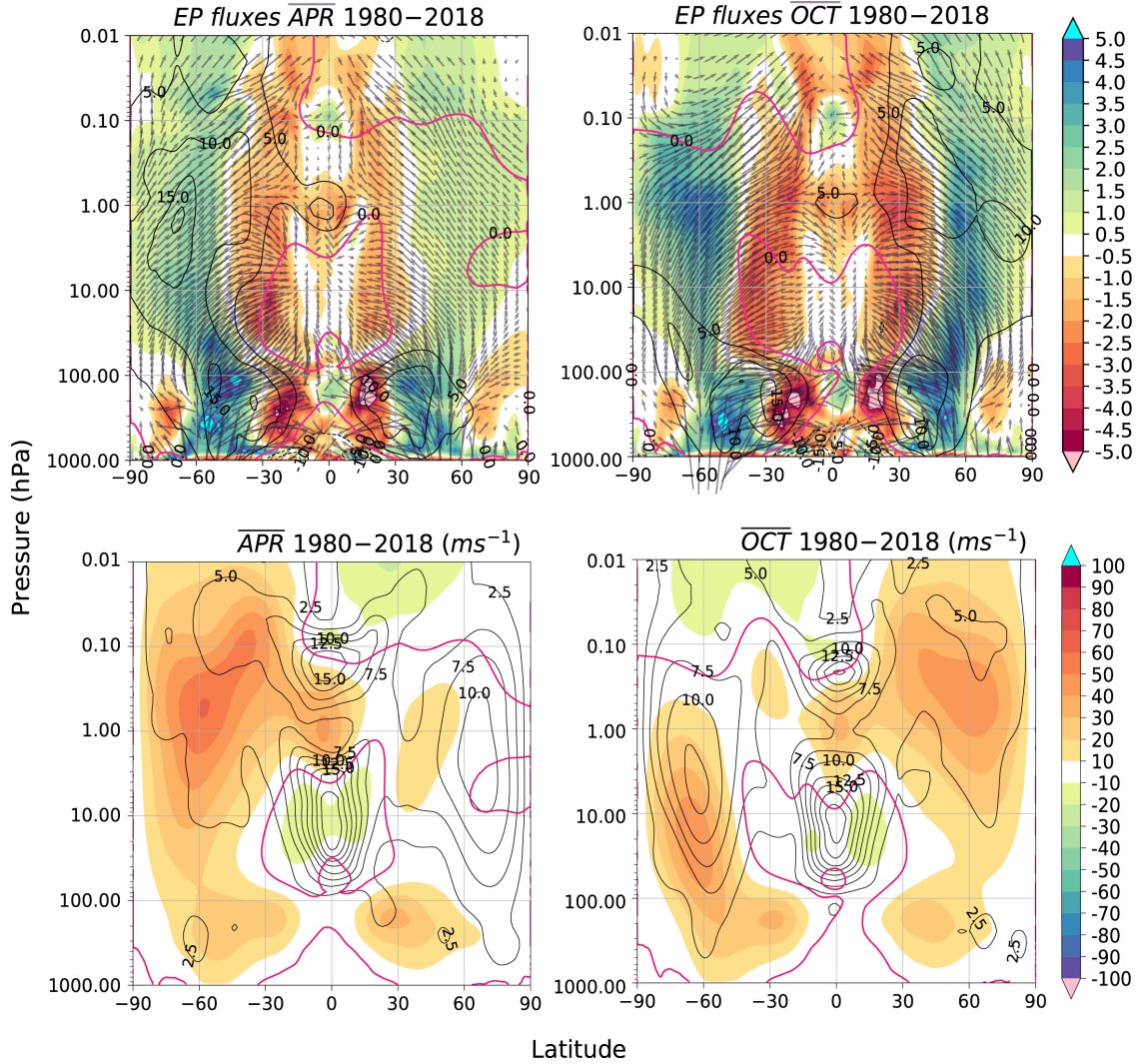


Figure 2. (upper row) Climatological E-P fluxes, calculated using daily U, V and T data over 1980-2018. Shading is the flux divergence with black contours the climatological winds. Negative U values are dashed and zero corresponds to the magenta contour. All quantities (E-P fluxes and U zonal winds) have been divided by the 1980-2018 standard deviation. The vectors below 100hPa have been appropriately thinned for display purposes. (lower row) Shading indicates the monthly climatological (1980-2018) U winds zonally averaged between 0° - 360° longitude. Negative (positive) wind values indicate easterly (westerly) flow. Black contours are the corresponding standard-deviations in ms^{-1} .

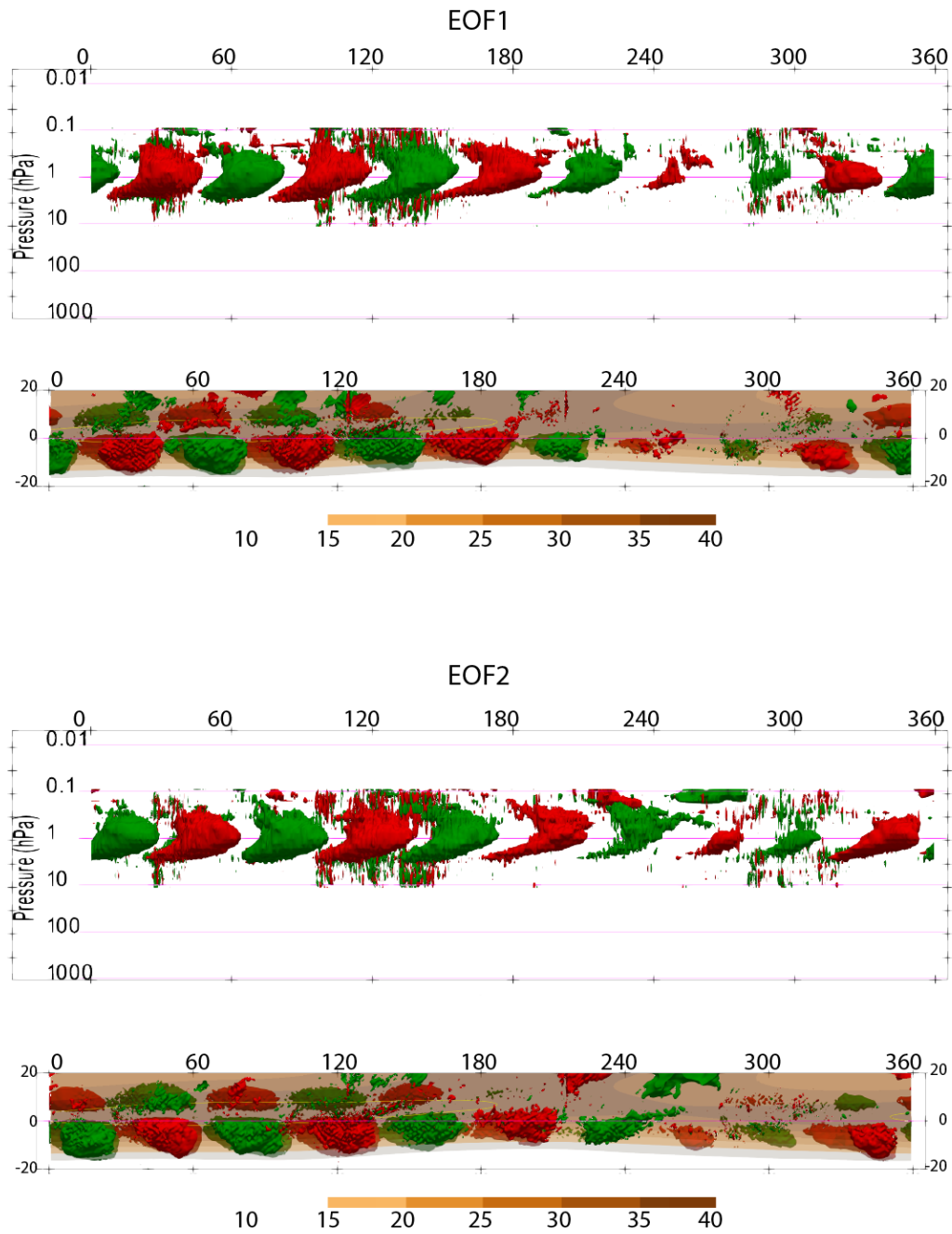


Figure 3. The leading 2 3D-EOFs of Q based on daily anomalies for April w.r.t. the climatological month viewed from the South and top-down. Positive (negative) Q values are indicated in red (green). Q isosurfaces correspond to $\pm 1.5e^{-11}$. The climatological U zonal wind velocities are the shaded background in the top-down view where velocities greater than 35ms^{-1} are identified by the yellow contour line. The opacity of the climatological U zonal wind values has been reduced in order to better see the structure below the 0.62hPa level.

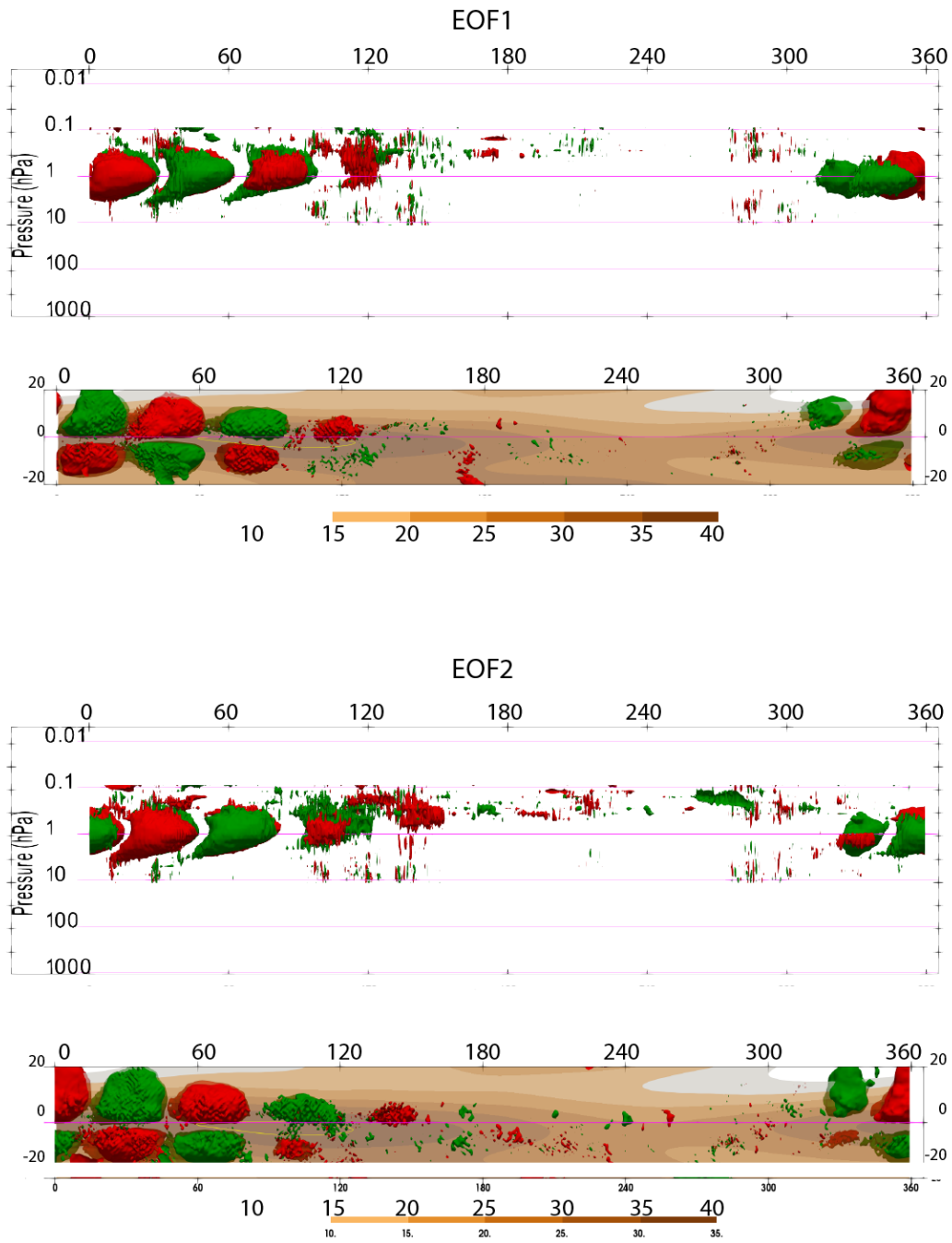


Figure 4. The leading 2 3D-EOFs of Q based on daily anomalies for October. Velocities greater than 30 m s^{-1} are identified by the yellow contour line. As for Figure 3, positive (negative) Q values are indicated in red (green). Q isosurfaces correspond to $\pm 1.5e - 11$.

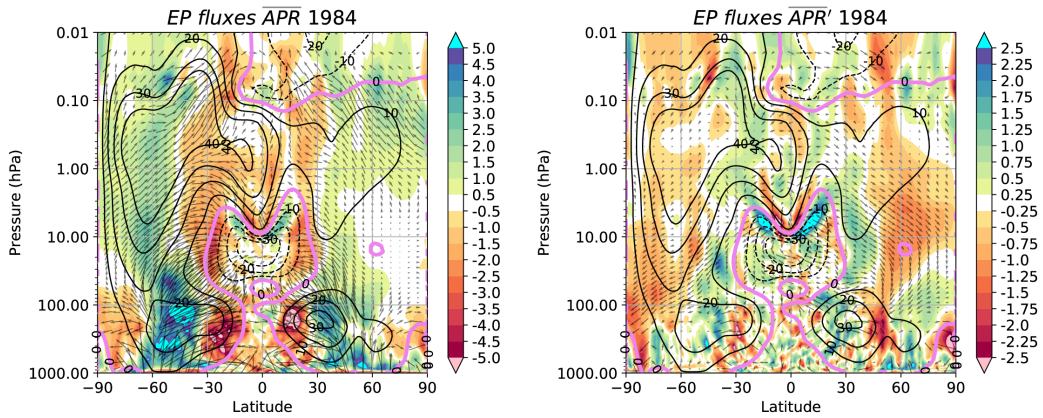


Figure 5. April 1984 monthly E-P fluxes (arrows) and flux divergence (shaded). Left panel is the average for April 1984, the right panel is the anomaly relative to long term 1980-2018 mean. Anomalies are normalised by the local standard deviation for the particular month. Black contours are respective monthly mean U zonal winds, and the zero contour (critical line) is shown in magenta (ms^{-1}).

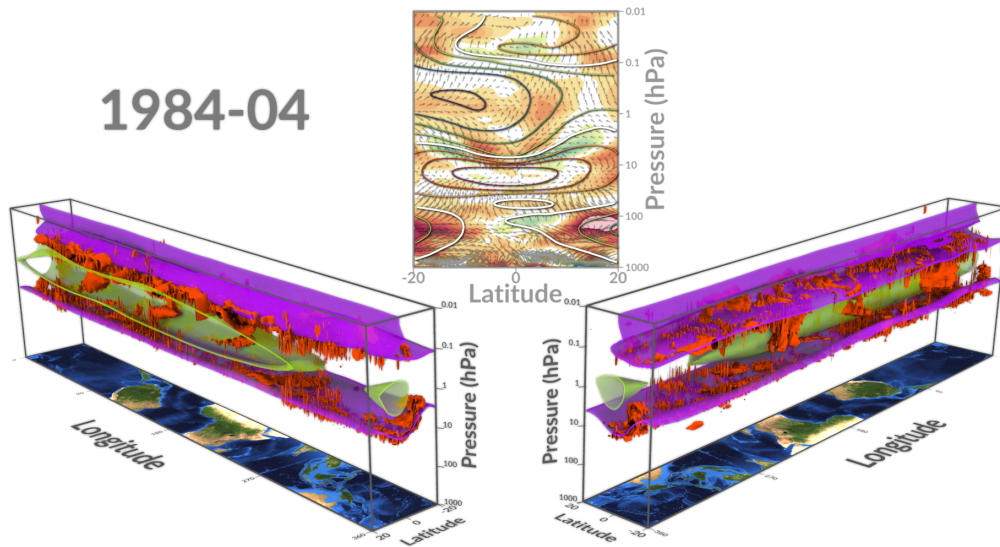


Figure 6. Isosurfaces of Q (positive $1.5e^{-11}$) and U (easterly $5ms^{-1}$ (magenta) and westerly $30ms^{-1}$ (green)) for April 1984. Q below 100hPa has been greyed-out. Isosurfaces are identified between 0.01hPa and 10hPa. The middle insert panel displays April 1984 monthly E-P fluxes (arrows) and flux divergence (shaded) between $20^{\circ}S$ and $20^{\circ}N$ with the critical line shown as the white contour.